Modeling whispering gallery mode III-V micro-lasers monolithically integrated on Silicon

S. Sant and A. Schenk

Integrated Systems Laboratory, ETH Zurich
Zurich, 8092, Switzerland.
{sasant & schenk}@iis.ee.ethz.ch

B. Mayer, S. Wirths, S. Mauthe, H. Schmid, and K. E. Moselund

IBM Zurich Research Laboratory
Rueschlikon, Switzerland
kmo@zurich.ibm.com

I. Introduction

The vision to speed up on-chip data communication by signal multiplexing using light and the promise to reduce the energy consumption of interconnects using optoelectronic devices has boosted on-chip photonics during the past years. Silicon is an ideal material for optical waveguides and passives, but due to the indirect band gap it is an inefficient emitter. Promising techniques to integrate III-V optoelectronic devices on Si were recently reported using selective area growth in trenches [1], in pre-patterned V-grooves [2], and using template assisted selective epitaxy (TASE) [3] all of which yield optically pumped micro-lasers. Geometric scaling of the photonic devices improves power efficiency due to reduced RC constant, but it is challenging to contact the scaled-down photonic devices. In this work, we employ coupled optoelectronic simulations to evaluate different paths for electrical pumping of our own optically pumped micro-lasers [3] while considering the constraints given by our process.

II. Characterization of GaAs Disk Lasers

Details on the fabrication of GaAs micro-disks by the TASE method are provided in Ref. [3]. Photoluminescence (PL) measurements were carried out on the micro-disk lasers. Room temperature (RT) PL spectra of the fabricated GaAs disk are shown in Fig. 1(a). For low excitation powers P_{th} < 17pJ/pulse, the device shows a broad emission centered around 879 nm. For pump powers > 17pJ/pulse, a strong peak emerges from the spontaneous emission background, giving rise to a non-linear increase of the peak-output power. The corresponding I/O curve is shown in Fig. 1(b) and reveals the characteristic S-shape, indicating low-threshold RT optically pumped lasing.

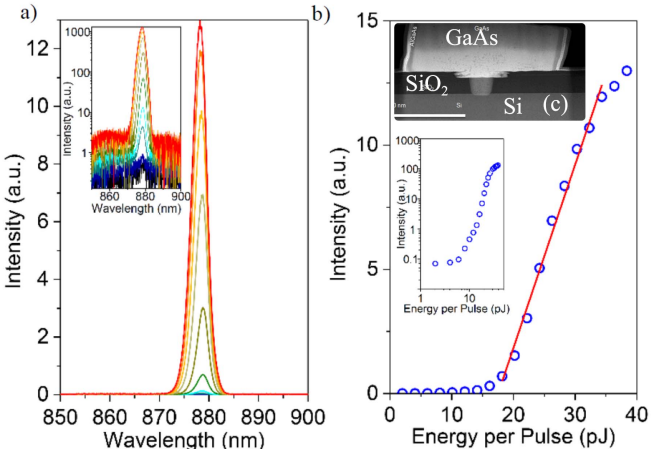

Figure 1: (a) PL at different optical actuation energy, (b) Peak intensity of the PL peak vs. optical pumping. (c) TEM image of GaAs micro-disk (data taken from [3]).

III. Optical Simulation of GaAs Disk

The cavity lifetime for the above micro-disk is calculated using Finite Difference Time Domain (FDTD) simulations as shown in Fig. 2. The simulated cavity lifetime of $\tau = 670$ fs corresponds to an end facet reflectivity of $R = 97\%$ and a Q factor of $Q = 730$. The optical mode is determined by simulating the time-dependent optical field profile in the micro-disk. To do so, randomly oriented dipole emitters simulating the exciton recombination are placed in the micro-disk, and the decay of the optical field is observed. After 1000 fs of simulation time, a clear mode profile as shown in Fig. 2(c) has evolved. This whispering gallery mode (WGM) can be identified by comparing the established mode profile from the FDTD simulations to the solutions of a Helmholtz equation solver. A similar mode profile is experimentally observed by recording the emission of a micro-disk above lasing threshold, as shown in Fig. 2(e). We conclude that the low-threshold RT operation of the device is a consequence of the high-order mode supported by the micro-disk and the high refractive index mismatch between SiO_2 and GaAs, providing

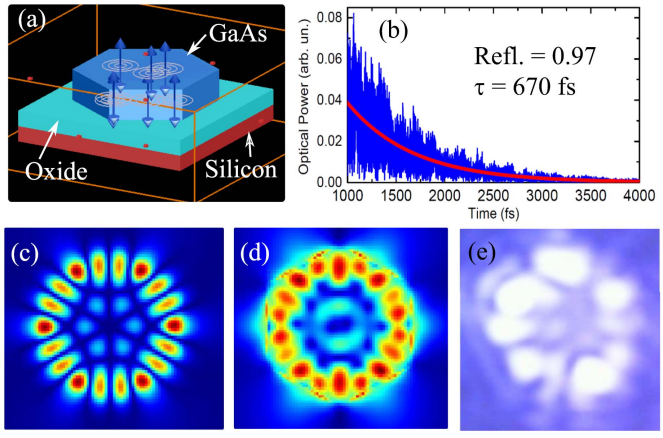

Figure 2: (a) GaAs disk structure simulated using FDTD solver. (b) Decay of energy with time. (c) Simulated time-averaged intensity profile at the center and (d) the top of the disk. (e) Image of the laser emission from a GaAs micro-disk.

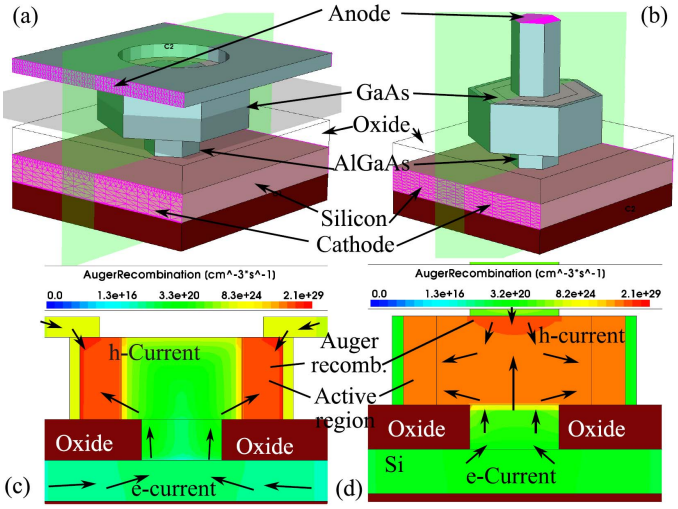

Figure 2: Proposed laser structure from hexagonal disk with (a) side contact – dev-A, and (b) top contact – dev-B. Colour-mapped diagram of the Auger recombination rate in vertical cut-planes (marked green) of (c) dev-A and (d) dev-B. The electron and hole current flow is marked by arrows. The lateral grey cut-plane of dev-A is used for the 2D simulations.

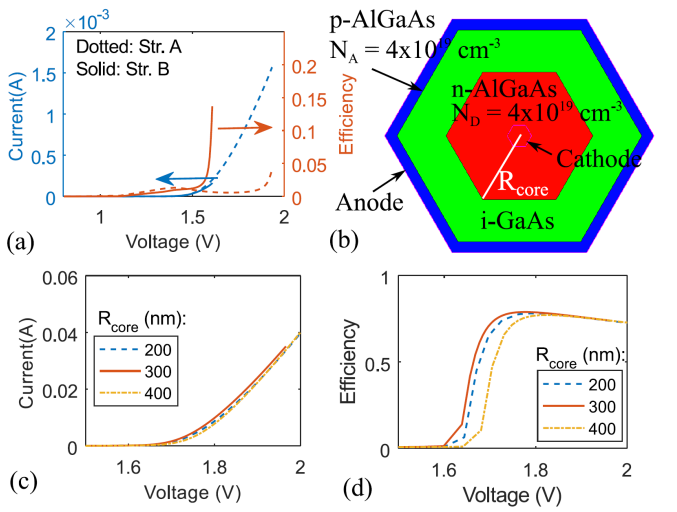

Figure 1:(a) I-V plots and efficiency of dev-A and dev-B plotted vs. applied bias. (b) Simplified 2D device geometry of the GaAs disk laser in Fig. 3(a), (c) I-V characteristics and (d) efficiency of the 2D laser showing that the lasing threshold is similar to that from the 3D simulations.

a sufficiently high cavity quality and low lasing threshold.

IV. Coupled Optoelectronic Simulations

The above results show the lasing potential of the GaAs disk at 300 K. To realize electrical pumping, the geometry of the device and the contacts must be designed to minimize their impact on the WGM. We developed two potential laser geometries based on the hexagonal disk (see Figs. 3(a) and 3(b)). Both types can be fabricated by etching an opening either along the periphery (dev-A) or at the center (dev-B) of the template oxide on the top of the disk, and epitaxially growing AlGaAs in the openings. FDTD simulations performed on these device structures confirm that the mode of Fig. 2(c) is again established. The simulations yield a reflectivity of 97.5% for dev-A and 98.7% for dev-B, respectively. The mode confinement in each of the structures is calculated from the time-averaged spatial intensity of the mode which yields 0.5 and 0.54 for dev-A and dev-B, respectively. Taking the above confinement and reflectivity as input, drift-diffusion simulations of the laser structures are performed using the TCAD simulator Sentaurus-Device. Calibrated models for doping-dependent mobility [4], band gap narrowing [5], SRH recombination [6], and Auger recombination [7] in GaAs are used. The temperature is assumed to be constant at 300 K throughout the devices.

Non-radiative recombination takes place by the SRH and Auger mechanisms, the latter being dominant. Figs. 3(c) and 3(d) suggest that the Auger rate is larger in dev-A compared to dev-B, due to high e-h densities at the edge of the top contact of dev-A. However, dev-B has the disadvantage that not the entire current passes through the active region. I-V characteristics of the devices along with the laser efficiency are plotted in Fig. 3(d). The 3D simulations do not converge after the onset of lasing. Yet, we can extract the lasing threshold from the converged I-V plots. It is 1.86 V and 1.55 V for dev-A and dev-B, respectively. The latter structure exhibits a lower lasing threshold as well as a higher laser efficiency at the lasing onset owing to the higher reflectivity and confinement factor, and the lower loss from Auger process.

Coupled optical-drift-diffusion simulations of a simplified 2-dimensional geometry of dev-A (Fig. 3(a)) were performed with S-Device to analyze the effect of a shrinking core radius of the AlGaAs layer. The WGM resembling mode in Fig. 2(c) is selected for the simulations. The device with $R_{core} = 300$ nm shown in Fig. 4(a) corresponds to the lateral cross section of the disk in Fig. 2(a). I-V and efficiency curves of the 2D devices with $R_{core} = 200$, 300, and 400 nm are plotted in Figs. 4(c) and 4(d), respectively. The efficiency of the laser is found to be 80%. Laser threshold and efficiency are insensitive to R_{core}. All the above simulations confirm that the given devices can be used as WGM lasers.

V. Conclusion

The micro-disk laser fabricated by TASE exhibits single mode operation and RT lasing due to the high refractive index mismatch to the SiO_2 template. Using the simulated optical mode profile of the lasing mode in drift-diffusion simulations demonstrates that vertically and laterally contacted device geometries could enable electrical pumping of the monolithically integrated devices.

References

[1] Wang, Z. et al. Nature Photonics 9, 837–842 (2015). [2] Norman, J. et al. Optics Express Vol. 25, 3927-3934 (2017). [3] Wirths et al, ACS Nano, 2018, 12 (3), p 2169. [4] Arora et al, IEEE Trans. Electron Devices vol. 29, p. 292. [5] Jain et. al. SSE, vol. 35, p. 639, 1992. [6] Hwang C. J., J. Appl. Phys., vol. 42, p. 4408 (1971). [7] Lush et al, J. Appl. Phys. Vol. 72, p. 1436.